

Direct Growth of Dense, Pristine Metal Nanoplates with Well-Controlled Dimensions on Semiconductor Substrates

Yugang Sun*

Center for Nanoscale Materials,
Argonne National Laboratory, 9700 South Cass Avenue,
Argonne, Illinois 60439

Received August 8, 2007

Revised Manuscript Received October 8, 2007

Shape-controlled synthesis of metal nanostructures has attracted intensive interest in the last several years because variation in morphologies of nanoparticles provides an effective means to fine tailor their properties.^{1–3} Various solution-phase chemical reactions have achieved great success in preparing metal nanoplates with the assistance of surfactant molecules, for instance, polymeric chains (e.g., poly(vinyl pyrrolidone) or PVP, polyamine),⁴ micellar assemblies (e.g., cetyltrimethylammonium bromide or CTAB, di(2-ethyl-hexyl) sulfosuccinate or AOT),^{5,6} coordinating ligands,⁷ biological reagents,⁸ etc. Some of these approaches have been extended to grow metal nanostructures with well-defined shapes on solid substrates. For example, seed-mediated synthetic processes with assistance of surfactants can grow gold nanorods on silicon⁹ or glass substrates¹⁰ and gold nanoplates on conductive indium tin oxide substrates.¹¹ However, the use of surfactant molecules for directing the anisotropic growth of metal nanoparticles somehow complicates the reaction systems. Most recently, Buriak and co-workers study the growth of metal nanostructures with various shapes (e.g., nanoinkshuks) on semiconductor substrates.¹² In this communication, we report a simple and

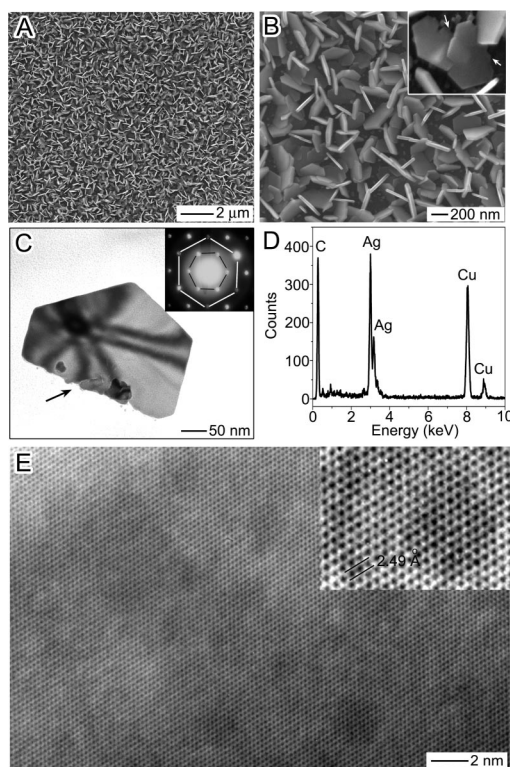
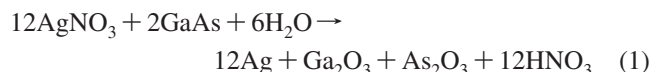


Figure 1. Characterization of Ag nanoplates formed at a reaction time of 2 min. (A) Low- and (B) high-magnification SEM images; (C) low- and (E) high-resolution TEM images; (D) EDX spectrum of Ag nanoplates on a TEM grid. The inset in (E) represents an enlarged image of a small area of (E), clearly showing lattice fringes with a periodicity of 2.49 Å. The arrows in (C) and inset of (B) highlight the roughness of the edges of the Ag nanoplates, which stick to the GaAs substrate. Reaction conditions: *n*-type (110) GaAs wafer with dopant (Si) concentration of $1.5 \times 10^{18} \text{ cm}^{-3}$; 1 M AgNO₃ aqueous solution; reaction temperature of $\sim 22^\circ \text{C}$.

surfactant-free approach to fast grow pristine metal nanoplates with well-controlled thicknesses and edge lengths on semiconductor wafers through galvanic reactions between pure aqueous solutions of metal salts and *n*-type semiconductor substrates.

For example, a typical synthesis of high-quality Ag nanoplates starts with cleaning a (110) *n*-GaAs wafer by dipping the wafer in a 2% hydrofluoric (HF) solution. **Caution:** *personal protective equipment is required to handle HF, which is highly corrosive toward tissues, bones in particular.* Placing a drop ($\sim 6 \mu\text{L}$) of aqueous solution of AgNO₃ (concentration of 1 M) on the surface of the cleaned wafer initiates the growth of Ag nanoplates at room temperature ($\sim 22^\circ \text{C}$) via a galvanic redox reaction



Continuous growth results in the formation of nanoplates with different sizes by controlling the reaction time. Images A and B in Figure 1 show low- and high-magnification scanning electron microscopy (SEM) images, respectively,

(12) Aizawa, M.; Cooper, A. M.; Malac, M.; Buriak, J. M. *Nano Lett.* **2005**, *5*, 815.

* E-mail: ygsun@anl.gov.

- (1) (a) El-Sayed, M. A. *Acc. Chem. Res.* **2001**, *34*, 257. (b) Wiley, B. J.; Im, S. H.; Li, Z.-Y.; McLellan, J.; Siekkinen, A.; Xia, Y. *J. Phys. Chem. B* **2006**, *110*, 15666. (c) Murphy, C. J.; Jana, N. R. *Adv. Mater.* **2002**, *14*, 80.
- (2) (a) Kottmann, J. P.; Martin, O. J. F.; Smith, D. R.; Schultz, S. *Phys. Rev. B* **2001**, *64*, 235402. (b) Jensen, T. R.; Kelly, L.; Lazarides, A.; Schatz, G. C. *J. Cluster Sci.* **1999**, *10*, 295. (c) Yin, Y.; Erdonmez, C.; Aloni, S.; Alivisatos, A. P. *J. Am. Chem. Soc.* **2006**, *128*, 12671.
- (3) (a) Kim, F.; Song, J. H.; Yang, P. *J. Am. Chem. Soc.* **2002**, *124*, 14316. (b) Krichevski, O.; Markovich, G. *Langmuir* **2007**, *23*, 1496.
- (4) (a) Sun, Y.; Mayers, B.; Xia, Y. *Nano Lett.* **2003**, *3*, 675. (b) Sun, X.; Dong, S.; Wang, E. *Langmuir* **2005**, *21*, 4710.
- (5) (a) Chen, S.; Carroll, D. L. *Nano Lett.* **2002**, *2*, 1003. (b) Chen, S.; Fan, Z.; Carroll, D. L. *J. Phys. Chem. B* **2002**, *106*, 10777.
- (6) (a) Maillard, M.; Giorgio, S.; Pileni, M.-P. *Adv. Mater.* **2002**, *14*, 1084. (b) Maillard, M.; Giorgio, S.; Pileni, M.-P. *J. Phys. Chem. B* **2003**, *107*, 2466.
- (7) Jin, R.; Cao, Y.; Mirkin, C. A.; Kelly, K. L.; Schatz, G. C.; Zheng, J. G. *Science* **2001**, *294*, 1901.
- (8) (a) Gugliotti, L. A.; Feldheim, D. L.; Eaton, B. E. *Science* **2004**, *304*, 850. (b) Rai, A.; Singh, A.; Ahmad, A.; Sastry, M. *Langmuir* **2006**, *22*, 736. (c) Liu, B.; Xie, J.; Lee, J. Y.; Ting, Y. P.; Chen, J. P. *J. Phys. Chem. B* **2005**, *109*, 15256.
- (9) (a) Mieszawska, A. J.; Slawinski, G. W.; Zamborini, F. P. *J. Am. Chem. Soc.* **2006**, *128*, 5622. (b) Liao, H.; Hafner, J. H. *J. Phys. Chem. B* **2004**, *108*, 19276.
- (10) Lee, K.-H.; Huang, K.-M.; Tseng, W.-L.; Chiu, T.-C.; Lin, Y.-W.; Chang, H.-T. *Langmuir* **2007**, *23*, 1435.
- (11) Umar, A. A.; Oyama, M. *Cryst. Growth Des.* **2006**, *6*, 818.

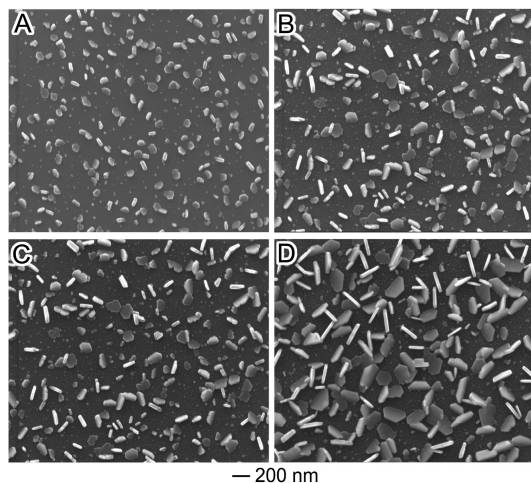


Figure 2. SEM images of Ag nanoplates formed at different growth times: (A) 5 s, (B) 15 s, (C) 30 s, and (D) 1 min. Other reaction conditions were the same as those given in Figure 1.

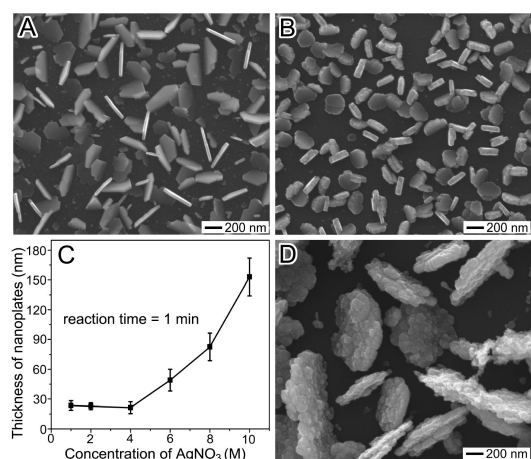


Figure 3. (A, B, D) SEM images of Ag nanostructures formed through reactions between *n*-type (100) GaAs wafers and (A) 1 M AgNO₃ for 2 min; (B) 6 M AgNO₃ for 1 min; and (D) 0.1 M AgNO₃ for 15 min. (C) Dependence of the thickness of the Ag nanoplates grown on *n*-type (100) GaAs wafers on the concentration of AgNO₃ after the reactions lasted 1 min. Reaction conditions were the same as those given in Figure 1 except that the GaAs wafers had a (100) surface orientation and dopant (Si) concentration of $\sim 1.0 \times 10^{18} \text{ cm}^{-3}$.

of a sample formed after the reaction lasts for 2 min. The images clearly show the formation of uniform nanoplates with high density (number of plates per unit of area = $2.82 \times 10^9 \text{ plates/cm}^2$) over the reaction area. The nanoplates have smooth surfaces and a thickness of $28 (\pm 5) \text{ nm}$ and edge lengths of 400–450 nm. They protrude from the surface plane of the substrate and have random orientations. Reactions on the wafers with different surface crystallographic orientations (e.g., (111) and (100) (see Figure 3A)) generate similar results, indicating that the formation of anisotropic Ag nanoplates is not induced by crystallographic epitaxy between GaAs and Ag. The crystallinity and composition of the nanoplates are characterized by the use of transmission electron microscopy (TEM) and energy-dispersive X-ray spectroscopy (EDX), respectively. Figure 1C presents a TEM image of an individual Ag plate sitting on a TEM grid against one of its flat surfaces. The edge (indicated by the arrow) that sticks to the GaAs wafer is rough, whereas the edges

out of the wafer surface are straight and sharp. This profile of the edges of the nanoplates is also confirmed by the SEM observations (inset of Figure 1B). The EDX curve (Figure 1D) recorded from an assembly of plates using a spectrometer equipped on TEM exhibits strong peaks of Ag as well as C and Cu (from the TEM grid). The absence of both Ga and As indicates that the GaAs substrate does not contaminate the as-grown Ag nanoplates. Selected-area electron diffraction pattern obtained by focusing the electron beam perpendicular to the flat surfaces of the plate (Figure 1C) is given in the inset of Figure 1C. The formation of hexagonal pattern indicates that the Ag nanoplates are crystallized in a face-centered cubic (fcc) lattice with the (111) flat surfaces. The same results have been observed for Ag plates synthesized in solution-phase reactions.^{4–8} The outer set of diffracted spots marked with white lines corresponds to a lattice spacing of 1.44 \AA and can be indexed to the {220} reflection of fcc silver. The inner set (marked with black lines) with a lattice spacing of 2.49 \AA is believed to originate from the $(1/3)\{422\}$ reflection that is normally forbidden by an fcc lattice. The lattice fringes of high-resolution TEM (HRTEM) image (Figure 1E) of the nanoplates also exhibit a periodicity of 2.49 \AA . The uniformity and continuity of the lattice fringes indicate the high level of crystallinity of the Ag nanoplates.

The growth of Ag nanoplates is monitored by examining the structures formed at different growth times. Figure 2 shows a series of SEM images of Ag structures that are generated by terminating the reactions at different times. Platelike structures with small sizes (edge lengths of $\sim 85 \text{ nm}$) are formed at an early stage, i.e., a reaction time of 5 s (Figure 2A). With increasing reaction time, the edge lengths of Ag nanoplates increase accordingly, whereas the thicknesses remain essentially constant. As a result, the size of Ag nanoplates grown via the simple approach described in this work can be easily tuned by controlling the reaction time. The thicknesses of the plates are determined by the lateral dimensions of the nuclei formed at a very short reaction time. Research to understand the fast nucleation process and how the crystalline structures of the nuclei affect the growth process is ongoing.

As mentioned previously, crystalline orientations of the surfaces of the GaAs substrates exhibit a negligible effect on the morphology and crystallinity of Ag nanoplates. Figure 3A shows an SEM image of Ag nanoplates formed on an *n*-type GaAs wafer with (100) surface orientation and a dopant (Si) concentration of ca. $1.0 \times 10^{18} \text{ cm}^{-3}$ after the wafer reacts with a 1 M aqueous AgNO₃ solution for 2 min. The results show that the Ag structures formed on GaAs wafers with (100) and (110) surface orientations are essentially identical except for the minor difference in density ($1.99 \times 10^9 \text{ plates/cm}^2$ for (100) wafer versus $2.82 \times 10^9 \text{ plates/cm}^2$ for (110) wafer) of nanoplates. Detailed studies indicate that the difference in density of nanoplates is ascribed to the difference in dopant concentrations of the GaAs substrates rather than their surface orientations.

The concentration of AgNO₃ also influences the morphologies and lateral parameters of Ag nanoplates. An increase in the concentration of AgNO₃ solutions leads to an increase

in the thickness of the as-grown Ag nanoplates. Figure 3B shows an SEM image of the nanoplates obtained by reacting with 6 M AgNO₃ (on a (100) GaAs wafer) for 1 min, indicating the significant increase in thickness of the nanoplates in comparison to those obtained with 1 M AgNO₃ (Figure 3A). The dependence of the thicknesses of the nanoplates (formed through reactions for 1 min) on the concentration of AgNO₃ is plotted in Figure 3C. When the concentration of AgNO₃ is lower than 4 M (and higher than 1 M), the nanoplates have essentially similar thicknesses, i.e., around 25 nm. The thicknesses of the plates increase with the concentration of AgNO₃ at concentrations higher than 4 M. The results indicate that the thicknesses of the Ag nanoplates can be easily tuned in the range of ~25–150 nm by controlling the concentration of AgNO₃. On the other hand, reaction with 0.1 M AgNO₃ solution generates nanoplates with rough surfaces rather than smooth surfaces. Such effects of concentration of AgNO₃ imply that deposition of silver atoms to the basal surfaces of the Ag nanoplates is a kinetically controlled process. A higher concentration of AgNO₃ provides a higher driving force to grow silver atoms on the lowest-energy (111) surfaces of the Ag nanoplates to thicken them. When the concentration of AgNO₃ is lower than a critical value, the driving force for depositing Ag atoms onto the basal planes of the plates is not enough to generate continuous lattices and smooth surfaces, resulting in the formation of nanoplates with rough surfaces (Figure 3D).

In addition, nanoplates made of metals other than Ag can be achieved through this strategy. For example, Pd nanoplates (see the Supporting Information, Figure S1) are prepared on an *n*-type (110) GaAs wafers by choosing appropriate precursors of palladium, i.e., 0.1 M Na₂PdCl₄ aqueous solution. In addition to GaAs, other semiconductor materials that can react with metal ions can also induce the galvanic reactions to form metal nanoplates. For instance, Ag nanoplates are formed on *n*-type (100) Si wafers (doped with P/Boron and wafer resistivity of 0–100 Ω m) after the wafers react with 1 M AgNO₃ for 30 min (see the Supporting Information, Figure S2). Although the quality of these nanoplates is worse than the Ag nanoplates grown on the *n*-GaAs wafers, they might be improved by carefully selecting the formula and concentration of precursors. The results indicate that the galvanic reactions on the surfaces of semiconductor wafers provide a versatile and powerful means to grow pure metal nanoplates on substrates.

The galvanic reaction between AgNO₃ and GaAs (eq 1) generates oxides, i.e., Ga₂O₃ (which might be dissolved in water under the experimental conditions) and As₂O₃, which are confirmed by Raman spectroscopy (see the Supporting Information, Figure S3). Although strong acid, i.e., HNO₃, is produced in the reaction, its concentration is too low to dissolve the as-grown As₂O₃, because only a small percentage of AgNO₃ is consumed to form Ag nanoplates. On the other hand, when 2% HF is added to the AgNO₃ solution, Ag crystals with sizes of several micrometers and irregular shapes that are much different from those shown in Figure 1 are formed on GaAs wafers. In this case, oxides are simultaneously dissolved by HF. These results indicate that

the layers of oxides play an important role in assisting the growth process of Ag nuclei into nanoplates with high anisotropy. A thin layer of oxides is generated and covered on the surface of a GaAs wafer once the reaction starts and Ag nuclei are formed. The existence of an oxide layer might prevent the nuclei from spreading in the surface of the wafer, resulting in the anisotropic growth of nanoplates standing out of the wafer surface. Because of the amorphous and porous properties of the oxide layer, the growing plates can access and stick on the surface of the wafer through the pores of the oxide layer. As a result, the edges of the nanoplates that contact the wafer are rough (inset of panels B and C in Figure 1). In addition, the existence of an oxide layer prevents the GaAs lattices from directly contacting Ag ions. Therefore, further reaction for growing the Ag nuclei (or small plates) into large plates is mainly dominated by a hole injection process in which each Ag⁺ injects a hole (i.e., positive charge) into the lattice of the GaAs wafer through the Ag nuclei (or small plates), because the reduction potential of Ag⁺/Ag ($E_{\text{Ag}^+/\text{Ag}}$) is higher than the surface valence band of the GaAs at the concentrations of the AgNO₃ solutions used in the experiments (see the Supporting Information, Figure S4A).¹³ Each silver ion releases a hole (h^+) at the edge surfaces (which have higher surface energy than the (111) basal surfaces) of a small plate (or nucleus) to convert itself to a Ag atom. The hole travels through the Ag particle and injects into the lattice of the GaAs wafer to react with GaAs with the assistance of water (from the AgNO₃ solution), resulting in the formation of oxides (see the Supporting Information, Figure S4B).

In summary, high-quality metal nanoplates with chemically clean surfaces and well-controlled dimensions have been synthesized through fast and simple galvanic reactions between semiconductor wafers and aqueous solutions of metal precursors. The cleanliness of the surfaces of the metal nanoplates is beneficial to the modification of the nanoplates with interesting molecules. For example, thiophenol molecules can form self-assembled monolayers on the surfaces of Ag nanoplates as shown in Figure 1 and the Ag nanoplates exhibit a strong enhancement in the Raman signal of the thiophenol molecules (see the Supporting Information, Figure S5). The metal nanoplates synthesized through the approach described in this work could find many applications, such as surface-enhanced Raman scattering (SERS), surface-enhanced fluorescence, catalysis, etc.

Acknowledgment. The work was supported by Department of Energy, Office of Science, Office of Basic Energy Sciences, under Contract DE-AC02-06CH11357. The electron microscopy was partially accomplished at the Electron Microscopy Center for Materials Research at Argonne National Laboratory, supported under Contract DE-AC02-06CH11357.

Supporting Information Available: Experimental information, full acknowledgment, and Figures S1–S5 (PDF). This material is available free of charge via the Internet at <http://pubs.acs.org>.

CM7022407

- (13) (a) Mandler, D.; Bard, A. J. *Langmuir* **1990**, *6*, 1489. (b) Allongue, P.; Blonkowski, S. J. *Electroanal. Chem.* **1991**, *317*, 77. (c) Allongue, P.; Blonkowski, S.; Souteyrand, E. *Electrochim. Acta* **1992**, *37*, 781.